Distributed Cooperative Control of Microgrid Storage

Thomas Morstyn, *Student Member, IEEE,* Branislav Hredzak, *Senior Member, IEEE,* and Vassilios G. Agelidis, *Senior Member, IEEE*

***Abstract*—This paper proposes dynamic energy level balancing between distributed storage devices as a strategy to improve frequency regulation and reliability in droop controlled microgrids. This has been achieved with a distributed multi-agent cooperative control system which modifies the output power of droop controlled storage devices so that they reach a balanced energy state. As the storage devices approach a common energy level they are able to contribute their full power capacity to deal with generation and demand fluctuations in the microgrid. The cooperative control system also provides secondary frequency control, restoring the microgrid to the reference frequency. Simulations have been completed showing that the cooperative control system improves frequency regulation compared to traditional droop control strategies when the storage devices begin at different energy levels and the microgrid experiences generation or demand variability. A control input saturation constraint has been developed which ensures that the cooperative control system will not overload the storage devices.**

***Index Terms*—Battery energy storage systems (BESS), distributed cooperative control, microgrid, multi-agent systems.**

I. Introduction

CURRENTLY, there is a trend away from the traditional model of centralised power generation towards smaller renewable generation sources distributed throughout the power network [1]. Microgrids have been proposed as a solution to the challenges presented by distributed intermittent renewable generation sources [2].

Energy storage (ES) devices can be used to balance the generation from intermittent sources with the demand from varying loads [3]. Power sharing between the ES devices, proportional to their power capacities, can be achieved with the well-known droop control method [4]. Droop control allows inverter connected ES devices to mimic the operation of conventional generators, which reduce their frequency to increase their real power output when additional power is required in the microgrid [5]. The microgrid frequency falls until the real power demand is matched by the combined real power output of the ES devices. This allows power sharing between the ES devices without requiring time critical communication links.

The traditional droop control method relies on the assumption of an inductive power network and thus non-ideal impedances of the ES devices and transmission lines can degrade power sharing accuracy. This can be mitigated by incorporating virtual output impedances into the ES device control systems [4].

Droop control has several additional limitations when used to facilitate power sharing between microgrid ES devices. Since power is proportionally shared between the ES devices in accordance with their power capacities rather than their energy levels, it is expected that those with lower initial energy levels will run out of energy first. Once an ES device is empty, it can no longer contribute its power capacity to maintaining the grid frequency during periods of high demand. If the power demand rises above the power capacity of the remaining ES devices the microgrid frequency limits will be violated and the remaining ES devices will be overloaded. Similarly, if an ES device becomes full then it can no longer absorb power during periods of excess supply, wasting the generation potential of renewable energy sources.

To prevent ES devices from prematurely running out of energy, the droop control strategy can be modified so that the power provided by the ES devices is weighted in inverse proportion to their energy level [5]. ES devices with less remaining energy provide less power, and thus the ES devices approach a balanced energy state as they empty. However, an undesirable aspect of this strategy is that the droop characteristics of the ES devices are dependent on their energy levels rather than their power capacities. As the ES devices run out of energy they reduce the amount of power used to maintain the microgrid frequency, so frequency regulation deteriorates. Further, since power is predominantly shared amongst ES devices with higher energy levels, some ES devices may be overloaded even when the total power demand is below the combined power capacities of the ES devices.

Centralised control systems can be used to optimally control power network ES devices [6], [7]. However, a centralised control system introduces a single point of failure.

Distributed control systems address these issues and present advantages in terms of robustness, extensibility and flexibility over centralised control systems [8]. A control system is considered distributed if it is made up of autonomous agents connected by a communication network, each independently pursuing their own control objective utilising only local information and information from their neighbours [9]. Multi-agent control systems have been applied to economic dispatching [10], secondary voltage control [11] and distributed secondary frequency control [12] in microgrids.

This paper proposes dynamic energy level balancing between ES devices as a strategy to improve frequency regulation and reliability in droop controlled microgrids. This has been

T. Morstyn, B. Hredzak and V. G. Agelidis are with the Australian Energy Research Institute and the School of Electrical Engineering and Telecommunications, University of New South Wales (UNSW Australia), Sydney, NSW 2052 Australia (email: t.morstyn@student.unsw.edu.au, b.hredzak@unsw.edu.au, vassilios.agelidis@unsw.edu.au).

achieved with a distributed control system based on multi-agent cooperative control. The cooperative control system modifies the traditional droop control power sharing method so that the microgrid ES devices use neighbour to neighbour communication to reach a balanced energy level. The cooperative control system incorporates distributed secondary frequency control between the ES devices restoring them to the microgrid reference frequency while maintaining accurate load sharing between them in steady state. A control signal saturation constraint has been developed which ensures the cooperative control system will not overload the microgrid ES devices.

Simulations have been completed showing that the proposed cooperative control system provides improved frequency regulation over the energy weighted droop control strategy when ES devices begin at different energy levels and the microgrid experiences generation or demand variability. Since the cooperative control system acts as a modification to traditional droop control, proper power sharing and frequency regulation will be maintained even in the event of communication failures, and in networks with droop controlled generators or ES devices which are not part of the communication network.

This paper is organised as follows. Section II discusses microgrid droop control. Section III provides the battery and inverter models used to design the cooperative control system. Section IV describes the cooperative control system design procedure and discusses the cooperative control signal saturation constraint. The performance of the proposed cooperative control system is verified through simulations in Section V. Section VI concludes the paper.

II. Microgrid Droop Control

Battery energy storage systems (BESS) can be used to provide controllable microgrid storage. Each BESS consists of a battery and a four quadrant inverter allowing control of the real and reactive power it injects or absorbs from the microgrid [13]. To maintain network stability, the BESS must be controlled to balance the difference between power generation and demand in the microgrid. This can be accomplished with the droop control method, which also provides power sharing between the BESS.

The BESS inverter can be modelled as a controllable AC voltage source $V_i\angle\delta$ connected to the microgrid through an output impedance $Z\angle\theta$. Let the microgrid common coupling bus voltage be $V_b\angle 0^\circ$. Assuming the inverter control system includes suitable virtual impedance so that its overall output impedance is highly inductive, $Z\angle\theta \approx jX$ [4]. If the inverter voltage angle δ is relatively small, the real and reactive output powers can be approximated as

$$P \approx \frac{V_i V_b}{X}\delta \text{ and } Q \approx \frac{V_i(V_i - V_b)}{X}. \tag{1}$$

These approximations motivate the standard droop control equations for controlling the inverter voltage frequency and magnitude [4],

$$\omega = \omega^* - m_p(P - P^*),\ V_i = V^* - n_q(Q - Q^*). \tag{2}$$

In these equations ω^* and V^* are the references for the microgrid voltage frequency and magnitude, m_p and n_q are the real and reactive power droop coefficients, and P^* and Q^* are the real and reactive power references, which are achieved when the microgrid voltage frequency and magnitude match the reference values. When the microgrid is islanded the difference between the total microgrid power demand and the combined reference powers is shared between the inverters in inverse proportion with their droop coefficients.

Selection of the droop coefficients presents a trade-off between voltage regulation and the required inverter output power. The droop control coefficients should be chosen taking into account power quality standards specified by the relevant utility. For example the Australian Energy Market Operator (AEMO) specifies a maximum long term frequency range of 49.5Hz to 50.5Hz for islanded operation [14] and a voltage magnitude range of -6% to +10% [15].

To make full use of the BESS power capacities to maintain the voltage frequency and magnitude, the droop coefficients should be set so that [4]

$$m_p = \frac{\omega_{\max} - \omega_{\min}}{2P_{\max}},\ n_q = \frac{V_{\max} - V_{\min}}{2Q_{\max}}. \tag{3}$$

In these equations $[\omega_{\min},\ \omega_{\max}]$ and $[V_{\min},\ V_{\max}]$ are the allowed operating ranges of the voltage frequency and magnitude and $P_{\max}$ and $Q_{\max}$ are the real and reactive power capacities of the BESS. The factors of 2 in the denominator of these equations arise based on the assumption that the BESS can both absorb and inject its full real and reactive power capacities.

Since the traditional droop control does not take the BESS energy levels into account, BESS with lower initial energy levels are expected to run out of energy first. To prevent this an energy weighted droop control strategy can be used. The real power contribution of each BESS is reduced in proportion to their energy level so that they will reach their minimum energy level at the same time [4]. The real droop control equation is modified so that

$$\omega = \omega^* - \frac{m_p}{\alpha}(P - P^*) \tag{4}$$
$$\alpha = \max\left(\frac{E - E_{\min}}{E_{\max} - E_{\min}},\ 0.01\right).$$

In these equations E is the current BESS energy and $E_{\max}$ and $E_{\min}$ are the battery energy limits. The value of α is limited at 0.01 to prevent $\frac{m_p}{\alpha}$ going to infinity. When the BESS device is full $\alpha = 1$ and the full inverter real power capacity is utilised.

Adjusting the droop coefficients based on the energy level of the BESS prevents the full inverter real power capacity from being utilised for frequency regulation. In this paper a distributed cooperative control structure utilising neighbour to neighbour communication is proposed to achieve a balanced energy level among the BESS while allowing the droop controlled BESS to make full use of their power capacities. In Section V it is shown that the proposed cooperative control system is able to balance the BESS energy levels, provides improved frequency regulation over the energy weighted droop control strategy (4) and prevents the BESS from being overloaded during periods of high demand.

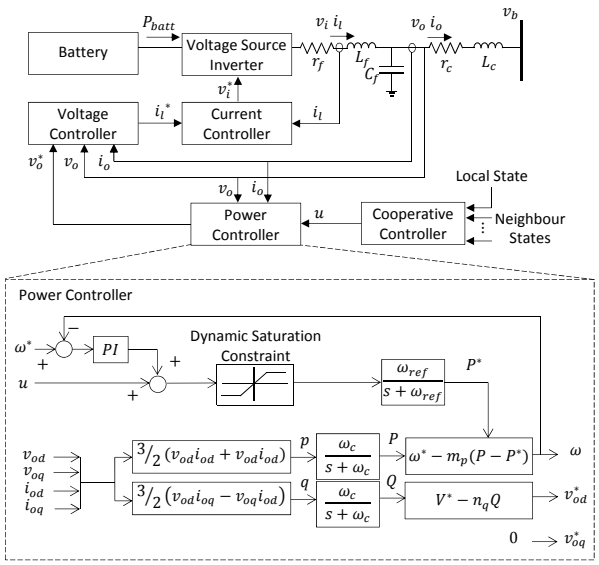

Fig. 1. Droop controlled BESS with cooperative control.

III. Battery Energy Storage System

A block diagram of a BESS is shown in Fig. 1. The BESS incorporates a battery, a voltage source inverter, an LC output filter, a grid connection impedance, and the inverter control system.

The BESS provides real power to the microgrid by drawing energy from a battery. With a suitably designed LC filter the inverter can be modelled as an ideal three phase AC voltage source providing the input voltage of the LC filter [16]. A series resistance and inductance are used to model the impedance of the cable and transformer connecting the BESS to the microgrid.

The BESS includes a closed loop power controller, voltage controller and current controller [16]. Droop control is implemented by the power controller which sets the BESS reference output voltage frequency and magnitude. The droop control power reference is modified by a cooperative controller to achieve energy level balancing between the BESS and to regulate the microgrid frequency to the reference frequency.

In this paper, the cooperative controller is designed based on cooperative state variable feedback control, assuming each BESS has access to its full state, and the states of its neighbours in the sparse communication network. Full state information allows linear quadratic regulator design to be used to generate a cooperative control law, and provides a simple stability condition for the global system dynamics, as shown in Section IV. In the case of incomplete state information it may still be possible to maintain the proposed control strategy, with the addition of a suitable cooperative observer, as addressed in [9].

A. BESS Small Signal Modelling

The BESS dynamics are described by a 15 state small signal state space model. Small signal models were derived for the modified power controller (12) and battery energy dynamics (14). These were combined with small signal models for the voltage controller (15), current controller (16), LC output filter and grid connection impedance (17) from [16] to obtain the overall BESS small signal model. The BESS dynamics are formulated in a direct-quadrature (d-q) reference frame which rotates synchronously with the BESS frequency [17].

The cooperative controller generates a scalar control signal u based on the difference between the local agent state vector and the state vector received from its neighbours to achieve dynamic energy level balancing between the BESS and to provide secondary frequency control.

Let x be the BESS state vector,

$$x = \begin{bmatrix} \Delta E & \Delta P & \Delta Q & \Delta P^* & \Delta\psi & \Delta\phi_{dq} \\ \Delta\gamma_{dq} & \Delta i_{ldq} & \Delta v_{odq} & \Delta i_{odq} \end{bmatrix}^T, \quad (5)$$

where E is the battery energy level, P and Q are filtered real and reactive power measurements, P^* is the droop control real power reference, ψ is the secondary frequency controller integral state, ϕ_{dq} and γ_{dq} are the d and q axis voltage and current controller integral states, and i_{ldq}, v_{odq} and i_{odq} are the inverter filter input current, output voltage and output current d-q components. The overall small signal state space model for the BESS is given by

$$\dot{x} = Ax + Bu. \quad (6)$$

The state space matrices A and B are shown in equation (7).

B. Power Controller

The power controller is shown in Fig. 1. The real and reactive instantaneous output powers are calculated from the output voltage and current [16].

$$p = \frac{3}{2}(v_{od}i_{od} + v_{oq}i_{oq}),\ q = \frac{3}{2}(v_{od}i_{oq} - v_{oq}i_{od}) \quad (8)$$

Low pass filters with cut-off frequency ω_c are used to obtain the fundamental components of the real and reactive power for the droop control [16]

$$P = \frac{\omega_c}{s+\omega_c}p,\ Q = \frac{\omega_c}{s+\omega_c}q. \quad (9)$$

To obtain the desired frequency and magnitude for the inverter output voltage, the droop control equations (2) are used. The microgrid reference voltage magnitude V^* is used as the reference for the direct component for the output voltage magnitude. The quadrature output voltage reference is set to zero. The reactive power reference is set to zero so that reactive power will be shared between the BESS in proportion with their reactive power capacities.

A PI secondary frequency controller calculates the offset necessary to correct the frequency error resulting from the droop control. This signal is added to the cooperative control signal and filtered to produce the droop control real power reference. In steady state, the cooperative controller will ensure that the BESS share a common droop control real power reference, so that accurate power sharing is maintained between them.

Real power sharing between the BESS is provided by their frequency droop characteristic. The BESS droop control real

$$A = \begin{bmatrix} 0_{1\times1} & B_{E2}D_{c1}D_{v1}C_{pv} & B_{E2}D_{c1}C_v & B_{E2}C_c & B_{E1}+B_{E2}(D_{c1}D_{v2}+D_{c2}) \\ 0_{4\times1} & A_p & 0_{4\times2} & 0_{4\times2} & B_p \\ 0_{2\times1} & B_{v1}C_{pv} & 0_{2\times2} & 0_{2\times2} & B_{v2} \\ 0_{2\times1} & B_{c1}D_{v1}C_{pv} & B_{c1}C_v & 0_{2\times2} & B_{c2}+B_{c1}D_{v2} \\ 0_{6\times1} & B_{LCL1}D_{c1}D_{v1}C_{pv}+B_{LCL2}C_{p\omega} & B_{LCL1}D_{c1}C_v & B_{LCL1}C_c & A_{LCL}+B_{LCL1}(D_{c1}D_{v2}+D_{c2}) \end{bmatrix} \quad (7)$$

$$B = \begin{bmatrix} 0 & 0 & 0 & \omega_{ref} & 0 & 0 & 0 & 0 & 0 & 0 & 0 & 0 & 0 & 0 & 0 \end{bmatrix}^T$$

power references are adjusted on a slower time-scale to return the microgrid to the reference frequency and to provide energy level balancing between them. A low pass reference filter is applied to the cooperative control signal and secondary frequency control signal to provide this decoupling. The transfer function between the cooperative control signal and the output power can be obtained from the BESS small signal state space model (7). The reference filter cut-off frequency ω_{ref} and secondary frequency PI controller gains $K_{p\omega}$ and $K_{i\omega}$ act as control parameters in this transfer function. In [18] it was shown that applying linear control system design techniques to this transfer function allows a desirable transient response to be obtained, while maintaining system stability.

The state equations for the droop control real power reference filter and secondary frequency control are given by

$$P^* = \frac{\omega_{\text{ref}}}{s+\omega_{\text{ref}}}(u + K_{p\omega}(\omega^* - \omega) + K_{i\omega}\psi) \quad (10)$$

$$\psi = \frac{1}{s}(\omega^* - \omega). \quad (11)$$

The power controller small signal model is given by

$$\begin{bmatrix} \dot{\Delta P} \\ \Delta Q \\ \Delta P^* \\ \Delta\psi \end{bmatrix} = A_p \begin{bmatrix} \Delta P \\ \Delta Q \\ \Delta P^* \\ \Delta\psi \end{bmatrix} + B_u u + B_p \begin{bmatrix} \Delta i_{ldq} \\ \Delta v_{odq} \\ \Delta i_{odq} \end{bmatrix} \quad (12)$$

$$\begin{bmatrix} \omega \\ v^*_{odq} \end{bmatrix} = \begin{bmatrix} C_{p\omega} \\ C_{pv} \end{bmatrix} \begin{bmatrix} \Delta P \\ \Delta Q \\ \Delta P^* \\ \Delta\psi \end{bmatrix}$$

$$A_p = \begin{bmatrix} -\omega_c & 0 & 0 & 0 \\ 0 & -\omega_c & 0 & 0 \\ \omega_{\text{ref}} m_p K_{p\omega} & 0 & -\omega_{\text{ref}}(1+m_p K_{p\omega}) & \omega_{\text{ref}} K_{i\omega} \\ m_p & 0 & -m_p & 0 \end{bmatrix}$$

$$B_u = \begin{bmatrix} 0 \\ 0 \\ \omega_{\text{ref}} \\ 0 \end{bmatrix},\ B_p = \frac{3\omega_c}{2} \begin{bmatrix} 0 & 0 & I_{od} & I_{oq} & V_{od} & V_{oq} \\ 0 & 0 & I_{oq} & -I_{od} & -V_{oq} & V_{od} \\ 0 & 0 & 0 & 0 & 0 & 0 \\ 0 & 0 & 0 & 0 & 0 & 0 \end{bmatrix}$$

$$C_{p\omega} = \begin{bmatrix} -m_p & 0 & m_p & 0 \end{bmatrix},\ C_{pv} = \begin{bmatrix} 0 & -n_q & 0 & 0 \\ 0 & 0 & 0 & 0 \end{bmatrix}.$$

C. Battery

The first order battery model from [13] is used to model the dynamics of the BESS energy level. The battery energy level state equation is given by

$$\dot{E} = -\frac{3}{2}(v_{id}i_{ld} + v_{iq}i_{lq}). \quad (13)$$

The battery small signal state space model is given by

$$\begin{bmatrix} \dot{\Delta E} \end{bmatrix} = B_{E1} \begin{bmatrix} \Delta i_{ldq} \\ \Delta v_{odq} \\ \Delta i_{odq} \end{bmatrix} + B_{E2} \begin{bmatrix} \Delta v_{idq} \end{bmatrix} \quad (14)$$

$$B_{E1} = -\frac{3}{2} \begin{bmatrix} V_{id} & V_{iq} & 0 & 0 & 0 & 0 \end{bmatrix}$$

$$B_{E2} = -\frac{3}{2} \begin{bmatrix} I_{ld} & I_{lq} \end{bmatrix}.$$

D. Voltage Controller

The small signal model for decoupled d–q axis PI voltage controllers with feed forward current gain is provided by [16].

$$\begin{bmatrix} \dot{\Delta\phi_d} \\ \Delta\phi_q \end{bmatrix} = B_{v1} \begin{bmatrix} \Delta v^*_{odq} \end{bmatrix} + B_{v2} \begin{bmatrix} \Delta i_{ldq} \\ \Delta v_{odq} \\ \Delta i_{odq} \end{bmatrix} \quad (15)$$

$$\begin{bmatrix} \Delta\ i^*_{ld} \\ \Delta\ i^*_{lq} \end{bmatrix} = C_v \begin{bmatrix} \Delta\phi_d \\ \Delta\phi_q \end{bmatrix} + D_{v1} \begin{bmatrix} \Delta v^*_{odq} \end{bmatrix} + D_{v2} \begin{bmatrix} \Delta i_{ldq} \\ \Delta v_{odq} \\ \Delta i_{odq} \end{bmatrix}$$

$$B_{v1} = \begin{bmatrix} 1 & 0 \\ 0 & 1 \end{bmatrix}\ B_{v2} = \begin{bmatrix} 0 & 0 & -1 & 0 & 0 & 0 \\ 0 & 0 & 0 & -1 & 0 & 0 \end{bmatrix}$$

$$C_v = \begin{bmatrix} K_{iv} & 0 \\ 0 & K_{iv} \end{bmatrix}\ D_{v1} = \begin{bmatrix} K_{pv} & 0 \\ 0 & K_{pv} \end{bmatrix}$$

$$D_{v2} = \begin{bmatrix} 0 & 0 & -K_{pv} & -\omega^* C_f & F & 0 \\ 0 & 0 & \omega^* C_f & -K_{pv} & 0 & F \end{bmatrix}$$

E. Current Controller

The small signal model for decoupled d–q axis PI current controllers is provided by [16].

$$\begin{bmatrix} \dot{\Delta\gamma_d} \\ \Delta\gamma_q \end{bmatrix} = B_{c1} \begin{bmatrix} \Delta i^*_{ldq} \end{bmatrix} + B_{c2} \begin{bmatrix} \Delta i_{ldq} \\ \Delta v_{odq} \\ \Delta i_{odq} \end{bmatrix} \quad (16)$$

$$\begin{bmatrix} \Delta\ v^*_{id} \\ \Delta\ v^*_{iq} \end{bmatrix} = C_c \begin{bmatrix} \Delta\gamma_d \\ \Delta\gamma_q \end{bmatrix} + D_{c1} \begin{bmatrix} \Delta i^*_{ldq} \end{bmatrix} + D_{c2} \begin{bmatrix} \Delta i_{ldq} \\ \Delta v_{odq} \\ \Delta i_{odq} \end{bmatrix}$$

$$B_{c1} = \begin{bmatrix} 1 & 0 \\ 0 & 1 \end{bmatrix} \quad B_{c2} = \begin{bmatrix} -1 & 0 & 0 & 0 & 0 & 0 \\ 0 & -1 & 0 & 0 & 0 & 0 \end{bmatrix}$$

$$C_c = \begin{bmatrix} K_{ic} & 0 \\ 0 & K_{ic} \end{bmatrix} \quad D_{c1} = \begin{bmatrix} K_{pc} & 0 \\ 0 & K_{pc} \end{bmatrix}$$

$$D_{c2} = \begin{bmatrix} -K_{pc} & -\omega^* L_f & 0 & 0 & 0 & 0 \\ \omega^* L_f & -K_{pc} & 0 & 0 & 0 & 0 \end{bmatrix}$$

F. LC Filter and Grid Connection

The small signal model for the LC filter and grid connection is provided by [16].

$$\begin{bmatrix} \Delta\dot{i}_{ldq} \\ \Delta\dot{v}_{odq} \\ \Delta\dot{i}_{odq} \end{bmatrix} = A_{LCL} \begin{bmatrix} \Delta i_{ldq} \\ \Delta v_{odq} \\ \Delta i_{odq} \end{bmatrix} + B_{LCL1} \begin{bmatrix} \Delta v_{idq} \end{bmatrix} + B_{LCL2} \begin{bmatrix} \Delta\omega \end{bmatrix} \tag{17}$$

$$A_{LCL} = \begin{bmatrix} -\frac{r_f}{L_f} & \omega^* & -\frac{1}{L_f} & 0 & 0 & 0 \\ -\omega^* & -\frac{r_f}{L_f} & 0 & -\frac{1}{L_f} & 0 & 0 \\ \frac{1}{C_f} & 0 & 0 & \omega^* & -\frac{1}{C_f} & 0 \\ 0 & \frac{1}{C_f} & -\omega^* & 0 & 0 & -\frac{1}{C_f} \\ 0 & 0 & \frac{1}{L_c} & 0 & -\frac{r_c}{L_c} & \omega^* \\ 0 & 0 & 0 & \frac{1}{L_c} & -\omega^* & -\frac{r_c}{L_c} \end{bmatrix}$$

$$B_{LCL1} = \begin{bmatrix} \frac{1}{L_f} & 0 \\ 0 & \frac{1}{L_f} \\ 0 & 0 \\ 0 & 0 \\ 0 & 0 \\ 0 & 0 \end{bmatrix} \quad B_{LCL2} = \begin{bmatrix} I_{lq} \\ -I_{ld} \\ V_{oq} \\ -V_{od} \\ I_{oq} \\ -I_{od} \end{bmatrix}$$

IV. Cooperative Control

BESS which are part of the cooperative control system are connected by a sparse communication network providing neighbour to neighbour communication.

The communication network can be described by a directed graph $\mathcal{G} = \{\mathcal{V}, \mathcal{E}\}$, where $\mathcal{V} = \{1, ..., N\}$ is the set of N nodes, each associated with a BESS, and $\mathcal{E}$ is the set of edges of the graph. An edge $(i, j) \in \mathcal{E}$ if there is a link allowing information to flow from node i to node j. Let the neighbours of node i be $\mathcal{N}_i$, where $j \in \mathcal{N}_i$ if $(j, i) \in \mathcal{E}$. Assume the graph is strongly connected, so there is a set of edges providing a path between every pair of nodes. Let the graph adjacency matrix be

$$\mathcal{A} = [a_{ij}] \in \mathbb{R}^{N \times N}, \tag{18}$$

$$a_{ij} = \begin{cases} 1, & (j, i) \in \mathcal{E} \\ 0, & \text{otherwise.} \end{cases}$$

For node i, the in-degree, $d_i = \sum_{j=1}^{N} a_{ij}$, and the out-degree, $d_i^o = \sum_{j=1}^{N} a_{ji}$. The graph is balanced if the in-degree of each node is equal to its out-degree. The graph degree matrix is given by $\mathcal{D} = \text{diag}(d_i)$ and the graph Laplacian matrix is given by $L = \mathcal{D} - \mathcal{A}$.

Assume there are N BESS connected by the communication graph with identical linear time-invariant (LTI) dynamics,

$$\dot{x_i} = Ax_i + Bu_i. \tag{19}$$

The cooperative control objective is for the BESS to reach a common energy level. This can be achieved with a local voting protocol where the control input depends on the difference between the local BESS state and the state of its neighbours. With the local voting protocol, the consensus reached by agents in a balanced communication graph is the average of their initial states [9]. Let the control input for node i be given by

$$u_i = cK \sum_{j \in \mathcal{N}_i} a_{ij}(x_j - x_i) \tag{20}$$

where $c > 0$ is a scalar coupling gain and K is the state variable feedback control matrix. The closed loop dynamics of the BESS are described by

$$\dot{x_i} = Ax_i + cBK \sum_{j \in \mathcal{N}_i} a_{ij}(x_j - x_i). \tag{21}$$

Let the global state vector for the graph be $\mathbf{x} = [x_1^T \ ... \ x_N^T]^T$. Then the overall global closed loop system dynamics are described by

$$\dot{\mathbf{x}} = [(I_N \otimes A) - cL \otimes BK]\mathbf{x}. \tag{22}$$

The stability properties of the global system dynamics depend both on the local BESS dynamics and the graph structure. The following cooperative control stability condition is provided by [9].

Let the eigenvalues of the graph Laplacian L be denoted $\lambda_i, \ i = 1, ..., N$. The global closed loop system dynamics (22) have stability properties equivalent to the stability properties of the systems

$$\dot{z_i} = (A - \lambda_i cBK)z_i, \ i = 1, ..., N. \tag{23}$$

Linear quadratic regulator design can be used to generate a state variable feedback control matrix K which minimises a quadratic cost function for each agent. The coupling gain c can then be chosen to guarantee system stability for any strongly connected communication graph [9].

The graph Laplacian L has a non-repeating zero eigenvalue $\lambda_i = 0$. Let $d_{\max}$ be the maximum in-degree of the graph. By the Geršgorin circle criterion all eigenvalues of L are located within a circle of radius $d_{\max}$, centred at $d_{\max}$ on the real axis of the complex plane. Therefore, the non-zero eigenvalues of L satisfy $\text{Re}(\lambda_i) > 0, \ i = 2, ..., N$ [9].

Let $Q \in \mathbb{R}^{N \times N}$ and $R \in \mathbb{R}$ be the positive definite Riccati design matrices. Consider a local control protocol $K = R^{-1}B^T P$, where P is the solution to the control algebraic Riccati equation

$$0 = A^T P + PA + Q - PBR^{-1}B^T P \tag{24}$$

Then the system Lyapunov equation for the systems in (23) is given by

$$(A - c\lambda_i BK)^* P + P(A - c\lambda_i BK) = -Q - (2c\,\text{Re}(\lambda_i) - 1)K^T RK. \tag{25}$$

It follows from Lyapunov theory that $A - c\lambda_i BK$ is Hurwitz if $c \geq \frac{1}{2\,\mathrm{Re}(\lambda_i)}$. Therefore, selecting $c \geq \frac{1}{2\,\min_i \mathrm{Re}(\lambda_i)}$, $i = 2, ..., N$ ensures the asymptotic stability of the systems

$$\dot{z_i} = (A + \lambda_i cBK)z_i,\ i = 2, ..., N \tag{26}$$

for the non-zero Laplacian eigenvalues, and the stability of the global closed loop system dynamics [9].

The state variable feedback gain matrix minimises the local agent cost function

$$J_i = \frac{1}{2}\int_0^\infty (x_i^T Q x_i + u_i^T R u_i)dt. \tag{27}$$

The design Riccati matrices Q and R can be selected to adjust the relative cost of state error and control effort. This allows the cooperative control system to be tuned to trade-off between the speed of energy convergence and the inverter output power used to achieve it. To ensure stability the coupling gain can be selected as

$$c = \max\left(\frac{1}{2\min_i \mathrm{Re}(\lambda_i)}, 1\right),\ i = 2, ..., N \tag{28}$$

where $\lambda_i,\ i = 2, ..., N$ are the non-zero eigenvalues of the communication graph Laplacian matrix L.

From (28) it can be seen that the minimum value of c to ensure stability is set by the non-zero graph Laplacian eigenvalue with the smallest real component. If the communication network between the BESS includes redundant links, the BESS may still be connected following communication link failure. The stability of the global system dynamics for sub-networks resulting from communication link failure can be assessed by checking whether the coupling gain requirement is still satisfied for the new Laplacian eigenvalues. Bounds on the graph Laplacian eigenvalues for different communication networks are provided in [19]. In the event of communication failure resulting in unconnected BESS, the secondary frequency control loops need to be disabled so that the microgrid steady state frequency deviation can be used to provide load sharing.

To prevent overloading and possibly damaging the BESS inverters, the control system needs to ensure the maximum output power capacity of the inverters is not exceeded. Without suitable constraints the combination of the power required to balance the microgrid demand with the additional power used to achieve dynamic energy level balancing could overload the BESS. The power controller includes a dynamic saturation constraint on the cooperative control signal to prevent this, as shown in Fig. 1.

Let $P_{\max}$ be the maximum real power capacity of the BESS inverter and P be the real output power of the inverter. To ensure the inverter is not overloaded the following condition should be satisfied by the power controller.

$$|P| \leq P_{\max} \tag{29}$$

The steady state droop control output power is given by [12],

$$P = \frac{\omega^* - \omega}{m_p} + P^*. \tag{30}$$

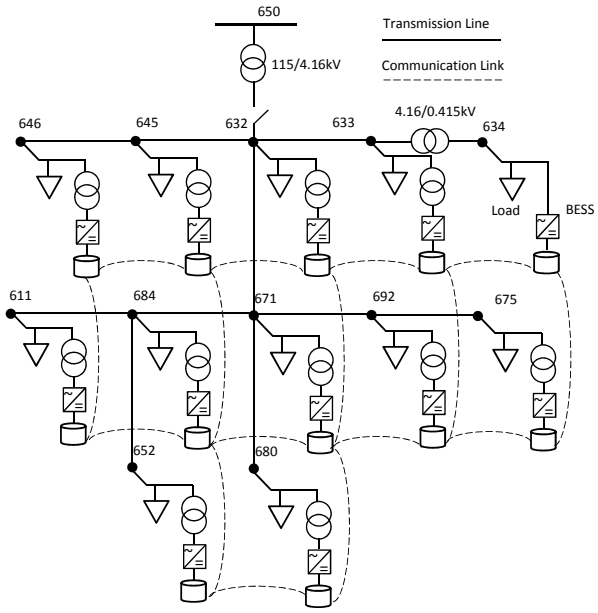

Fig. 2. Microgrid based on the IEEE 13 Bus Feeder. A communication graph with bidirectional links connects the BESS.

To ensure (29) the following constraint should be satisfied by P^*.

$$-P_{\max} - \frac{\omega^* - \omega}{m_p} \leq P^* \leq P_{\max} - \frac{\omega^* - \omega}{m_p} \tag{31}$$

This can be achieved by applying the following dynamic saturation constraints to the input of the droop control real power reference filter (10),

$$\begin{aligned} u + K_{p\omega}(\omega^* - \omega) + K_{i\omega}\psi &\leq P_{\max} - \frac{\omega^* - \omega}{m_p}, \\ u + K_{p\omega}(\omega^* - \omega) + K_{i\omega}\psi &\geq -P_{\max} - \frac{\omega^* - \omega}{m_p}. \end{aligned} \tag{32}$$

V. Case Studies

Simulations were carried out to demonstrate the performance of the proposed dynamic energy level balancing cooperative control system. First, a simulation is shown demonstrating the operation of the cooperative controller in an islanded microgrid with constant loads. Then, simulations are shown demonstrating the improvement the cooperative controller provides in terms of frequency regulation over the energy weighted droop control strategy (4) when there are variations in the net microgrid power demand.

The simulations were performed using an islanded microgrid based on the IEEE 13 Node Test Feeder [20], supported by twelve droop controlled BESS connected by a communication network, shown in Fig. 2. The microgrid is comprised of a 115kV high voltage (HV) substation, 11 4.16kV medium voltage (MV) buses and a 415V low voltage (LV) bus. The simulations have been carried out assuming that the microgrid has disconnected from the high voltage substation and thus must operate in islanded mode. The AEMO power quality requirements are used as performance criteria for the control

TABLE I
SIMULATION PARAMETERS

Battery		Voltage Controller	
E_{total}	200 kWh	K_{pv}	4.1497
E_{max}	160 kWh	K_{iv}	3.90×10^{3}
E_{min}	40 kWh	F	0.75
Power Controller		**Current Controller**	
P_{max}	100 kW	K_{pc}	0.7390
m_p	3.14×10^{-5}	K_{ic}	3.17×10^{4}
n_q	1.36×10^{-4}	**Output Filter & Grid Connection**	
ω^*	314.16 rad/s	L_f	0.0135 mH
V^*	$\sqrt{2}\times240V$	C_f	0.0029 F
ω_c	31.42 rad/s	r_f	0.05 Ω
ω_{ref}	3.142 rad/s	L_c	0.35 mH
$K_{p\omega}$	5×10^{5}	r_c	0.03 Ω
$K_{i\omega}$	1×10^{6}		

systems, imposing a frequency range of 49.5Hz to 50.5Hz [14] and a voltage magnitude range of -6% to +10% [15].

Each bus in the microgrid is connected to a feeder with a range of residential and industrial loads and distributed generation sources. These can be modelled as a single aggregated constant power load at each bus [21]. A BESS consisting of a 100kW inverter and a 200kWh lithium ion battery is connected to each of the 11 MV microgrid buses by an LV/MV transformer and to the single LV bus. The microgrid line impedances have been averaged across the three phases. The BESS parameters are provided in Table I.

A bidirectional communication network connecting each BESS to other nearby BESS has been used. The cooperative control system is not required for primary control of the microgrid and thus could be provided by existing telecommunication links, rather than requiring a specially designed industrial control network.

A. Case A: Cooperative control with dynamic input saturation constraint

To demonstrate the operation of the dynamic energy level balancing cooperative control system, a simulation was conducted with a 20kW 10kVAr constant load at each bus. To prevent significant lifetime deterioration of the 200kWh capacity lithium ion batteries they should be kept between 80% and 20% charge [13], giving an allowed energy range of 160kWh to 40kWh. For the simulation, the BESS begin with energy levels between 160kWh and 50kWh.

The Riccati design matrices Q and R set the relative cost of state error and control effort in the quadratic cost function (27) which is minimised by the state variable feedback control matrix K. Bryson's rule provides a guide for selecting the Riccati design matrices that gives the error of each state and the magnitude of each control signal a similar weight, despite them having different units [22]. The Riccati design matrix associated with the state error, Q, was set to

$$Q = \frac{1}{E_{\text{total}}^2} C_E^T C_E = 1.929 \times 10^{-18} C_E^T C_E \qquad (33)$$

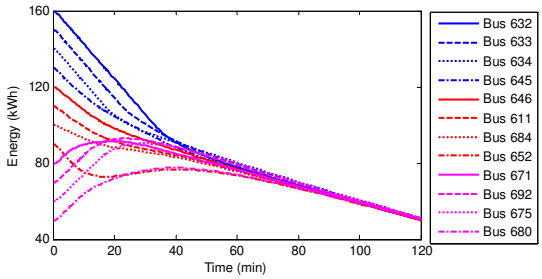

(a) Case A. BESS energy levels.

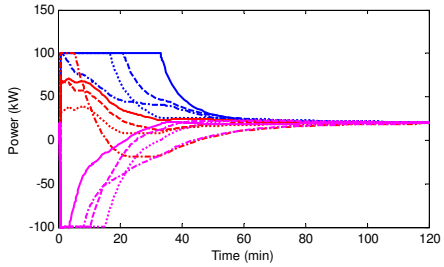

(b) Case A. BESS output powers.

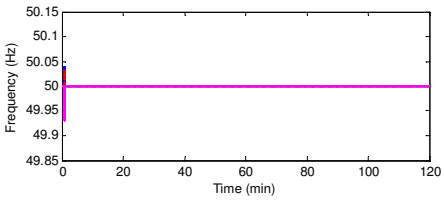

(c) Case A. BESS frequencies.

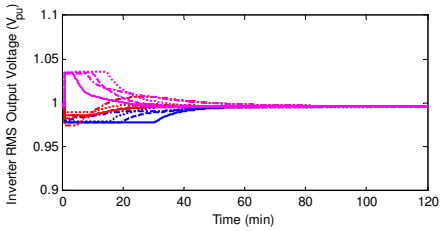

(d) Case A. BESS per unit RMS inverter output voltages.

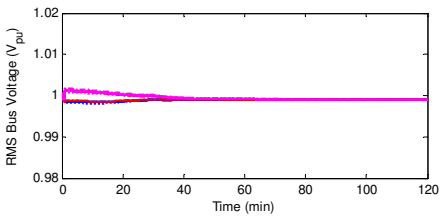

(e) Case A. BESS per unit RMS bus voltages.

Fig. 3. Case A. Cooperative control with dynamic input saturation constraint.

$$C_E = \begin{bmatrix} 1 & 0_{1\times14} \end{bmatrix}.$$

The selection of C_E means that of the 15 BESS states, only disagreement between the local BESS energy and the energy of its neighbours contributes to the cost function which is minimised by the state variable feedback controller.

The Riccati design matrix associated with the control effort

R was selected to compromise between the speed of energy balance and the inverter output powers.

$$R = 6.4 \times 10^{-15} \tag{34}$$

Following (28) the coupling gain was set to $c = 1$.

Fig. 3(a) shows that the BESS energy levels converge over two hours of operation. The dynamic cooperative control signal saturation constraint ensures the 100kW inverter power capacity is not exceeded, as shown in Fig. 3(b). Fig. 3(c) shows that the BESS frequencies vary between 49.93Hz and 50.04Hz before the secondary frequency control returns the microgrid to the reference frequency after 2.8s. As shown in Fig. 3(d), during energy balancing the inverter output voltages vary between 0.97pu and 1.04pu, well within the -6% to +10% microgrid voltage limits. The microgrid bus voltages vary between 0.998pu and 1.002pu, as shown in Fig. 3(e).

B. Case B: Cooperative control and traditional methods, frequency regulation comparison

This simulation demonstrates the improvement in frequency regulation which the cooperative control system can provide in islanded microgrids where generation and demand variability are expected. Consider the situation where the microgrid is islanded from the high voltage substation for two hours. Seven BESS begin fully charged at 160kWh and five begin with 90kWh. Initially, the load at each bus is 20kW and 10kVAr. A load spike, consisting of an additional 60kW load at each bus, occurs 90 minutes after islanding and lasts for 15 minutes. If the traditional droop control (2) is used the batteries which begin at 90kWh will run out of energy and the frequency limits will be violated. The energy weighted droop control strategy (4) prevents the BESS from running out of energy, but still fails to regulate the microgrid frequency.

Case B.1. presents the energy weighted droop control simulation and Case B.2. presents the cooperative control simulation.

1) Case B.1. Energy Weighted Droop Control: The energy weighted droop control strategy ensures that none of the BESS reach the minimum energy level of 40kWh over the two hours of islanded operation, as shown in Fig. 4(a). As the energy levels of the BESS decrease, their real power droop coefficient is increased according to (4). Less power is provided by the BESS with less energy, as shown in Fig. 4(b). This means that the total inverter output power capacity is not utilised to maintain the microgrid frequency within the 49.5Hz to 50.5Hz limits. Fig. 4(c) shows that the frequency droop in the microgrid increases over the low demand period, and when the demand spike occurs the low frequency limit of the microgrid is violated. Since the load power is predominantly provided by the BESS with higher energy levels these inverters are overloaded during the load spike.

2) Case B.2. Cooperative Control: The cooperative control system was applied using the same Riccati design matrices (33), (34) and coupling gain that were used for Case A. Fig. 5(a) shows that the BESS reach a common energy level after 60 minutes, so none of them reach the minimum energy level over the two hours. The maximum real output powers of the BESS are limited at the inverter capacity of 100kW by the dynamic saturation constraint, as shown in Fig. 5(b). The cooperative control system provides secondary frequency control maintaining the microgrid at the 50Hz reference frequency with a maximum frequency deviation of 0.11Hz, as shown Fig. 5(c). At the beginning and end of the load spike, transient frequency deviations of 0.001Hz are observed. The dynamic energy level balancing cooperative control system has successfully regulated the microgrid frequency and avoided overloading the BESS inverters. Comparing Fig. 4(d) and Fig. 5(d) it can be seen that under the cooperative control strategy, while the BESS are using their output powers to reach a balanced energy level, the inverter output voltages deviate by up to 0.043pu from the voltages observed during the energy weighted droop control case study. However, less voltage deviation between the BESS is observed once they have reached a balanced energy level since the load is shared equally between them. Fig. 5(d) and Fig. 5(e) show that the inverter output voltages and microgrid bus voltages are regulated within the microgrid voltage limits.

VI. Conclusion

In this paper it has been shown that the proposed strategy of dynamic energy level balancing between storage devices in droop controlled islanded microgrids provides improved frequency regulation over traditional droop control strategies when the storage devices begin at different energy levels and the microgrid experiences generation or demand variability. Dynamic energy level balancing has been achieved with a distributed multi-agent cooperative control system, offering advantages in terms of robustness, extensibility and flexibility over centralised control strategies. The cooperative control system provides distributed secondary frequency control, restoring the microgrid to the reference frequency. The cooperative control system design procedure guarantees system stability and allows the speed of energy convergence to be traded-off against the power used for energy level balancing. A control input saturation constraint has been developed which ensures that the cooperative control system will not overload the microgrid storage devices.

Promising directions for future work include the application of the proposed distributed energy level balancing control strategy to DC microgrids, along with extensions to the control strategy based on additional storage device objectives beyond energy balancing, such as lifetime maximisation.

References

[1] R. H. Lasseter, “Smart Distribution: Coupled Microgrids,” *Proceedings of the IEEE*, vol. 99, no. 6, pp. 1074–1082, Jun. 2011.

[2] R. Lasseter, “MicroGrids,” in *2002 IEEE Power Engineering Society Winter Meeting. Conference Proceedings (Cat. No.02CH37309)*, vol. 1, 2002, pp. 305–308.

[3] K. O. Oureilidis and C. S. Demoulias, “Microgrid wireless energy management with energy storage system,” in *2012 47th International Universities Power Engineering Conference (UPEC)*, Sep. 2012, pp. 1–6.

[4] J. M. Guerrero, J. C. Vasquez, J. Matas, L. G. de Vicuna, and M. Castilla, “Hierarchical Control of Droop-Controlled AC and DC Microgrids - A General Approach Toward Standardization,” *IEEE Transactions on Industrial Electronics*, vol. 58, no. 1, pp. 158–172, Jan. 2011.

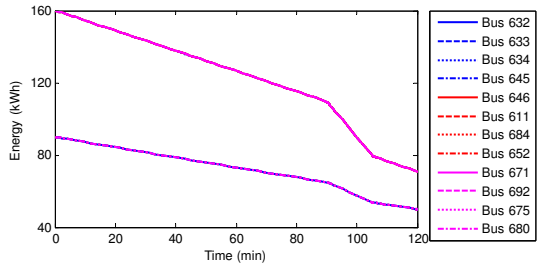

(a) Case B.1. Energy weighted droop control BESS energy levels.

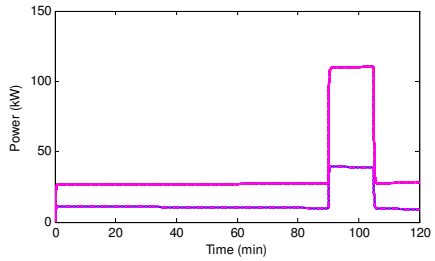

(b) Case B.1. Energy weighted droop control BESS output powers.

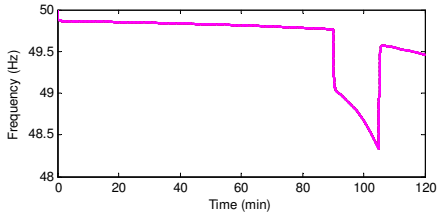

(c) Case B.1. Energy weighted droop control BESS frequencies.

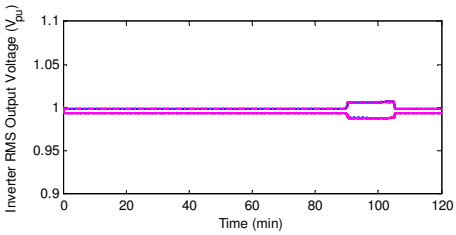

(d) Case B.1. Energy weighted droop control per unit RMS inverter output voltages.

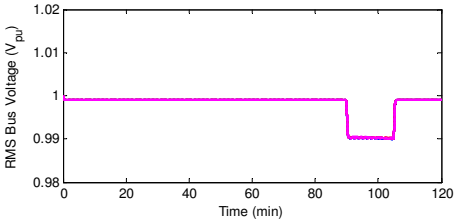

(e) Case B.1. Energy weighted droop control per unit RMS bus voltages.

Fig. 4. Case B.1. Frequency regulation comparison, energy weighted droop control.

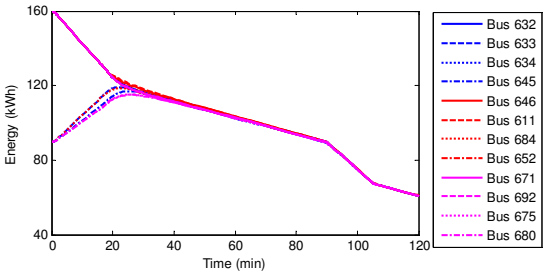

(a) Case B.2. Cooperative control BESS energy levels.

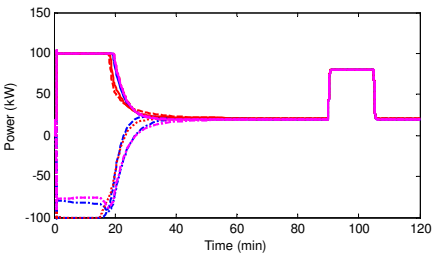

(b) Case B.2. Cooperative control BESS output powers.

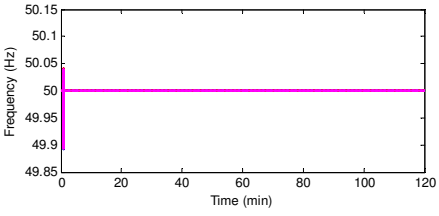

(c) Case B.2. Cooperative control BESS frequencies.

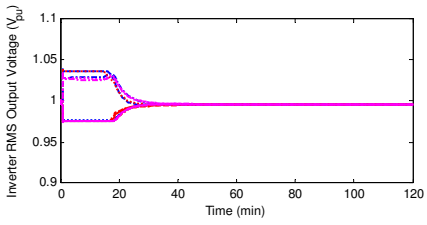

(d) Case B.2. Cooperative control per unit RMS inverter output voltages.

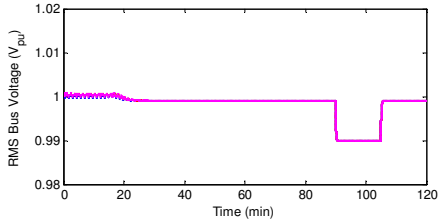

(e) Case B.2. Cooperative control per unit RMS bus voltages.

Fig. 5. Case B.2. Frequency regulation comparison, cooperative control.

[5] J. Guerrero, L. Garcia de Vicuna, J. Matas, M. Castilla, and J. Miret, "A Wireless Controller to Enhance Dynamic Performance of Parallel Inverters in Distributed Generation Systems," *IEEE Transactions on Power Electronics*, vol. 19, no. 5, pp. 1205–1213, Sep. 2004.

[6] X. Liu, A. Aichhorn, L. Liu, and H. Li, "Coordinated Control of Distributed Energy Storage System With Tap Changer Transformers for Voltage Rise Mitigation Under High Photovoltaic Penetration," *IEEE Transactions on Smart Grid*, vol. 3, no. 2, pp. 897–906, Jun. 2012.

[7] D. Gayme and U. Topcu, "Optimal power flow with large-scale storage

integration," *IEEE Transactions on Power Systems*, vol. 28, no. 2, pp. 709–717, May 2013.
[8] S. D. J. McArthur, E. M. Davidson, V. M. Catterson, A. L. Dimeas, N. D. Hatziargyriou, F. Ponci, and T. Funabashi, "Multi-Agent Systems for Power Engineering Applications-Part I: Concepts, Approaches, and Technical Challenges," *IEEE Transactions on Power Systems*, vol. 22, no. 4, pp. 1743–1752, Nov. 2007.
[9] F. L. Lewis, H. Zhang, K. Hengster-Movric, and A. Das, *Cooperative Control of Multi-Agent Systems*, ser. Communications and Control Engineering. London: Springer London, 2014.
[10] S. Kar and J. M. Moura, "Consensus + innovations distributed inference over networks: cooperation and sensing in networked systems," *IEEE Signal Processing Magazine*, vol. 30, no. 3, pp. 99–109, May 2013.
[11] A. Bidram, A. Davoudi, F. L. Lewis, and J. M. Guerrero, "Distributed Cooperative Secondary Control of Microgrids Using Feedback Linearization," *IEEE Transactions on Power Systems*, vol. 28, no. 3, pp. 3462–3470, Aug. 2013.
[12] J. W. Simpson-Porco, F. Dörfler, and F. Bullo, "Synchronization and power sharing for droop-controlled inverters in islanded microgrids," *Automatica*, vol. 49, no. 9, pp. 2603–2611, Sep. 2013.
[13] K. Le Dinh and Y. Hayashi, "Coordinated BESS control for improving voltage stability of a PV-supplied microgrid," in *2013 48th International Universities' Power Engineering Conference (UPEC)*, Sep. 2013, pp. 1–6.
[14] "Application of Frequency Operating Standards During Periods of Supply Scarcity," Reliability Panel, The Australian Energy Market Commission, Tech. Rep. April, 2009.
[15] B. Noone, "PV Integration on Australian distribution networks: Literature review," The Australian PV Association, Tech. Rep. September, 2013.
[16] N. Pogaku, M. Prodanovic, and T. C. Green, "Modeling, Analysis and Testing of Autonomous Operation of an Inverter-Based Microgrid," *IEEE Transactions on Power Electronics*, vol. 22, no. 2, pp. 613–625, Mar. 2007.
[17] M. Milosevic, "Decoupling control of d and q current components in three-phase voltage source inverter," Technical Report, ETH Zurich, Tech. Rep., 2003.
[18] J. Guerrero, J. Vasquez, J. Matas, M. Castilla, and L. de Vicuna, "Control Strategy for Flexible Microgrid Based on Parallel Line-Interactive UPS Systems," *IEEE Transactions on Industrial Electronics*, vol. 56, no. 3, pp. 726–736, Mar. 2009.
[19] C. W. WU, *Synchronization in Complex Networks of Nonlinear Dynamical Systems*. Singapore: World Scientific Publishing Co. Pte. Ltd., 2007.
[20] W. Kersting, "Radial distribution test feeders," in *2001 IEEE Power Engineering Society Winter Meeting. Conference Proceedings (Cat. No.01CH37194)*, vol. 2, pp. 908–912.
[21] S. Bolognani, G. Cavraro, F. Cerruti, and A. Costabeber, "A linear dynamic model for microgrid voltages in presence of distributed generation," in *2011 IEEE First International Workshop on Smart Grid Modeling and Simulation (SGMS)*, Oct. 2011, pp. 31–36.
[22] J. P. Hespanha, *Linear Systems Theory*. Princeton: Princeton University Press, 2009.

Thomas Morstyn (S'13) received the B.E. (Hon.) degree in electrical engineering from the University of Melbourne, Australia, in 2012.

He worked as an electrical engineer in the Rio Tinto Technology and Innovation group for two years. He is currently working towards the Ph.D. degree at the Australian Energy Research Institute, The University of New South Wales, Sydney, NSW, Australia. His current research interests include control systems for the integration of distributed renewable generation and storage into power networks.

Branislav Hredzak (M'98-SM'13) received the B.Sc./M.Sc. degree from the Technical University of Kosice, Slovak Republic, in 1993, and the Ph.D. degree from Napier University of Edinburgh, U.K., in 1997, all in electrical engineering.

He was a Lecturer and a Senior Researcher in Singapore from 1997 to 2007. He is currently a Senior Lecturer in the School of Electrical Engineering and Telecommunications, The University of New South Wales, Sydney, NSW, Australia. His current research interests include hybrid storage technologies and advanced control systems for power electronics and storage systems.

Vassilios G. Agelidis (S'89-M'91-SM'00) was born in Serres, Greece. He received the B.Eng. degree in electrical engineering from the Democritus University of Thrace, Thrace, Greece, in 1988, the M.S. degree in applied science from Concordia University, Montreal, QC, Canada, in 1992, and the Ph.D. degree in electrical engineering from the Curtin University, Perth, WA, Australia, in 1997.

From 1993 to 1999, he was with the School of Electrical and Computer Engineering, Curtin University. In 2000, he joined the University of Glasgow, Glasgow, U.K., as a Research Manager for the Glasgow-Strathclyde Centre for Economic Renewable Power Delivery. In addition, he has authored/co-authored several journal and conference papers as well as Power Electronic Control in Electrical Systems in 2002. From January 2005 to December 2006, he was the inaugural Chair of Power Engineering in the School of Electrical, Energy, and Process Engineering, Murdoch University, Perth. From December 2006 to June 2010, he was the Energy Australia Chair of Power Engineering at the University of Sydney. He is currently the Director of the Australian Energy Research Institute, The University of New South Wales, Sydney, NSW, Australia.

Dr. Agelidis received the Advanced Research Fellowship from the United Kingdoms Engineering and Physical Sciences Research Council in 2004. He was the Vice President Operations within the IEEE Power Electronics Society during 2006-2007. He was an Associate Editor of the IEEE POWER ELECTRONICS LETTERS from 2003 to 2005, and served as the Power Electronics Society (PELS) Chapter Development Committee Chair from 2003 to 2005. He was an AdCom Member of IEEE PELS for 2007-2009 and the Technical Chair of the 39th IEEE Annual Power Electronics Specialists Conference, Rhodes, Greece.